reduce the strength of inelastic hadronic particle-production rates, which are usually much smaller than the total rates of reaction (scattering). For this reason, the time scale of chemical equilibration is, in general, considerably longer than the thermal one.

6 Understanding collision dynamics

6.1 Cascades of particles

The principal shortcomings of the near-statistical-equilibrium method, combined with ideal flow of hadronic fluid in the study of heavy-ion collisions, are the following:

- we do not have a long-lived, large region of hot hadronic matter to look at, and some features of the collision are certainly not well equilibrated;
- we need to establish the physical conditions at the initial time τ_0; and
- the system considered is subject to rapid evolution and all thermal properties are actually fields, i.e., we have a position-dependent local temperature $T(\vec{x})$, etc.

Hence, a lot of effort continues to be committed to the development of a better understanding of the initial interaction dynamics, and its subsequent description within microscopic kinetic-scattering models. The research field of the study of computer-code 'event generators' is vast and undergoing development. Consequently, in this book, we will enter into discussion of kinetic models only as matters of example and/or principle. We survey the rapidly developing field in order to offer an entry point for further study.

For a novice in this very rapidly changing panorama, the best next step is to look at the progress of the working group which has been monitoring the development of the computer codes with the objective of ensuring that reasonable quality control is attained.

OSCAR (Open Standard Codes and Routines)[‖]. OSCAR begun in June 1997 to resolve the lack of common standards, documentation, version control, and accessibility in many transport codes. These transport codes for relativistic heavy-ion collisions differ from computer codes in other areas of physics, where numerical methods are only technical tools used to solve specific equations that define the physics. The source code of a nuclear-collision transport model often implements extra physical assumptions and dynamic mechanisms that go beyond the equations used to motivate its design. These algorithms often undergo evolution with time, and the very large number of phenomenological parameters also

[‖] See: *http://www-cunuke.phys.columbia.edu/people/molnard/mirror-OSCAR/oscar.*

https://doi.org/10.1017/9781009290753.009 Published online by Cambridge University Press

makes it difficult to pinpoint the relevant physical input controlling the observed computational result. Since the code itself defines the physical content of the model, it is essential to be able to closely scrutinize the actual algorithms used.

The list of codes currently either maintained or/and accessible, with the meaning of the acronyms, and principal authors is as follows**.

Correlation builders
CRAB – *Correlation After Burner*, by S. Prat.

Hydrodynamics
BJ-HYDRO – *Relativistic Hydrodynamics with Bjørken Geometry*, by A. Dumitru and D. H. Rischke.

Partonic/string transport
HIJING – *Heavy Ion Jet INteraction Generator*, by M. Gyulassy and X.-N. Wang [266].
HIJING/B-anti-B – *HIJING/Baryon Junction*, by S. Vance and M. Gyulassy.
MPC – *Molnar's Parton Cascade*, by D. Molnár.
neXus – by H.-J. Drescher and K. Werner.
PCPC – *Poincaré Covariant Parton Cascade*, by V. Boerchers, S. Gieseke, G. Martens, J. Meyer, R. Kammering and C. C. Noack.
VENUS – by K. Werner.
VNI – by K. Geiger, R. Longacre and D. Srivastava [130, 131].
VNIb – by S. A. Bass.
ZPC – *Zipping Parton Cascade*, by B. Zhang.

String/hadronic transport
ART – *Another Relativistic Transport*, by B.-A. Li and C.-M. Ko.
BEM – *Boltzmann Equation Model*, by P. Danielewicz.
BNC – *Burn and Crash*, by S. Pratt.
HSD – *Hadron String Dynamics*, by W. Cassing.
JAM –*Jet AA Microscopic Transport Model*, by Y. Nara.
JPCIAE – *Jetset Pythia CIAE (China Institute of Atomic Energy)*, by B.-H. Sa and A. Tai.
LEXUS – *Linear Extrapolation of ultra-relativistic Nucleon–Nucleon Scattering*, by S. Jeon.
LUCIAE – *Lund CIAE,*, by A. Tai and B.-H. Sa.
RQMD – *Relativistic Quantum Molecular Dynamics*, by H. Sorge [250].
UrQMD – *Ultra-relativistic Quantum Molecular Dynamics*, by S. A. Bass [274].

** For more details see *http://www-cunuke.phys.columbia.edu/people/molnard/mirror-OSCAR/oscar/models/list.html.*

https://doi.org/10.1017/9781009290753.009 Published online by Cambridge University Press

Transport tools
GCP – *General Cascade Program*, by Y. Pang.

PYTHIA, JETSET, and LUND, mentioned above, are programs for the generation of high-energy-physics events, i.e., for the description of collisions at high energies between elementary particles such as e^+, e^-, p, and $\bar{p}$ in various combinations. Together, they contain theory and models for a number of aspects of physics, including hard and soft interactions, parton distributions, initial- and final-state parton showers, multiple interactions, fragmentation, and decay.

Development of JETSET, the first member of the 'Lund Monte-Carlo' family, was begun in 1978. The most extensive of these programs is PYTHIA. Over the years, these two programs have more and more come to be maintained in common. In the most recent version, they have therefore been merged into one, under the PYTHIA label. The current version is PYTHIA 6.1, by T. Sjöstrand.[††]

The common feature within transport-cascade models is that they picture a multiscattering process as a succession of binary collisions and decays, each well separated in space–time. For such an approach to have a chance of success, we must be in a physical situation dominated by well-separated collisions, the so-called collision regime. It is rather easy to see where this collision regime will occur in nuclear collisions: the de Broglie wavelength of one of the incident particles, and its (classical) mean free path in the medium, have to be compared with each other in order to identify the collision partners.

For example, at low energy, the de Broglie wavelength can be as large as the radius of the nucleus, so the dynamics will be dominated by the scattering of all nucleons, not by two-body collisions. As the energy increases, the resolving power increases and one also crosses particle-production thresholds and enters the multiple-scattering process involving elastic and inelastic nucleon–nucleon collisions, as well as collisions between the hadrons produced. We call this energy region the 'hadronic-cascade' region; as extensive studies of the data show, at AGS energies, (10–15)A GeV, this is the dominant reaction mechanism. At higher energies, the de Broglie wavelength of the projectile becomes smaller than even a fraction of the size of a nucleon. The interaction will therefore involve the parton substructures – we reach the 'partonic-cascade' region.

In microscopic transport models describing the collision event (event generators), two primary mechanisms are used in order to describe evolution dynamics including production of particles: the nonperturbative production involving strong fields with field string-breaking, see Eq. (3.5),

[††] For more information, see *http://www.thep.lu.se/torbjorn/Pythia.html.*

https://doi.org/10.1017/9781009290753.009 Published online by Cambridge University Press

and the production due to reactions caused by collisions of individual particles:

- Programs using primarily measured and extrapolated hadronic cross sections, e.g., RQMD [250], ARC [202, 203], QGSM [83], and UrQMD [274].
- Programs using perturbative QCD reactions, e.g., VNI [130, 131] and HIJING [266]; the main differences between these two models are the following: VNI is a Monte-Carlo implementation of a parton-cascade model (PCM) in which the time evolution of heavy-ion collisions is simulated by the parton cascading, whereas HIJING assumes the Glauber theory in the description of A–A collisions and handles the soft process on the basis of the string model.
- There are also hybrid models such as the PHC [196], a parton–hadron-cascade model, which is an extension of the hadronic-cascade model incorporating hard partonic scattering based on HIJING. However, practically all generators mentioned have, in some ways, taken the hybrid approach.

The hadronic-event generators are more suitable for lower AGS energies, and can be extended to SPS energies by introducing novel reaction mechanisms. The partonic generators are more geared to RHIC and LHC energies, but again, with some fine tuning, can be applied to the SPS energies. The SPS energy range is so difficult to cover, since p-QCD seems not to be well defined at such 'soft' energies, but the hadron cascade alone clearly cannot describe this energy range properly. The hybrid model (PHC [196]) is therefore more able to handle that energy domain.

There are major uncertainties in the hadronic-cascade models related to the impossibility of measuring reaction all relevant cross sections, section 18.2, and the necessity to introduce particle-production mechanisms well beyond the scope of the model (color ropes, for example, in RQMD). The perturbative QCD reactions in the deconfined phase are, on other hand, well determined in terms of elementary processes. The major uncertainty arises from the soft-QCD properties: for small transfers of energy, the QCD processes become very strong, and the issue of what physical mechanism is indeed responsible for the soft cutoff arises. This is reminiscent of the fact that we do not understand, in terms of QCD, the (inelastic) low-energy processes: e.g., the inelastic N–N cross section. It is for this reason that considerable attention was given to the color-string mechanism of particle production, which can be tuned to describe very well the nucleon–nucleon inelastic interactions within the LUND family adaptation (see below) to nuclear collisions, the FRITIOF model [40, 205].

Unfortunately, both the scope and the extent of this introductory book do not allow us to pursue in detail how these approaches differ. The

https://doi.org/10.1017/9781009290753.009 Published online by Cambridge University Press

above remarks can, however, serve as an entry point to further reading, for an up-to-date report, see [271]. The reader should be aware that a book could be written just on the subject touched on the surface in this section.

In closing this discussion, we wish to note that it is of course of interest to check how far the microscopic dynamic models are leading to near-equilibrium thermal and chemical conditions. Several studies exploring particle production and momentum distributions have revealed a very good approach to chemical and thermal equilibrium [80, 249]. This result really confirms that the large nuclear-reaction system, at the energies considered, disposes of sufficiently many degrees of freedom, and that statistical near-equilibrium methods are able to characterize the final state reached in the reaction. These results do not imply that the conditions created in the event generator are those observed experimentally.

6.2 Relativistic hydrodynamics

In the hydrodynamic description of the evolution of matter, rather than individual particles, one considers the flow of particles in a volume element. Therefore, we consider as one of the dynamic equations the conservation of (e.g., baryon) number-density current, along with the conservation of energy–momentum flow. These flows are described in terms of the local flow field $\vec{v}(\vec{x}, t)$, or equivalently in terms of the 4-velocity vector of the flow u^μ:

$$\frac{dx^\mu}{d\tau} \equiv u^\mu(x) = \gamma(1, \vec{v}), \qquad \frac{dt}{d\tau} \equiv \gamma = \frac{1}{\sqrt{1 - \vec{v}^2}}. \tag{6.1}$$

We see that, in general,

$$u_\mu u^\mu \equiv u^2 = 1, \quad u_\mu = g_{\mu\nu} u_\nu. \tag{6.2}$$

We use Einstein's summation convention for repeated Greek indices (implied summation over time '0' and space '1, 2, 3'), and work in flat space–time $g_{\mu\nu} = g^{\mu\nu}$, with the metric convention $g^{\mu\nu} \equiv \mathrm{diag}(1, -1, -1, -1)$.

There is a simple relation between the 4-divergence of the 4-velocity and the 4-divergence of the density arising from the conservation of current. We write a conserved current j_μ in terms of the local density ρ:

$$\partial_\mu(\rho u^\mu) = \rho \partial_\mu u^\mu + u^\mu \partial_\mu \rho = 0, \qquad \partial_\mu = \frac{\partial}{\partial x^\mu}. \tag{6.3}$$

The proper time τ coordinate of the local volume element and laboratory frame coordinates are related by the Euler relation:

$$\frac{d}{d\tau} = u^\mu \partial_\mu = \gamma\left(\frac{\partial}{\partial t} + \vec{v} \cdot \vec{\nabla}\right), \qquad \partial_\mu = \left\{\frac{\partial}{\partial_t}, \vec{\nabla}\right\}. \tag{6.4}$$

https://doi.org/10.1017/9781009290753.009 Published online by Cambridge University Press

We divide Eq. (6.3) by ρ and obtain, using Eq. (6.4),

$$\boxed{\partial_\mu u^\mu = -\frac{1}{\rho_i}\frac{d\rho_i}{d\tau} \equiv \frac{1}{\tau^{\exp}}.} \tag{6.5}$$

We suggest, at the end of condition Eq. (6.5), that it is a suitable definition of the expansion life span of the system, Eq. (5.34). In fact, as Eq. (6.32) below is showing, this is exactly true (taking freeze-out proper time) for the case of longitudinal flow in one spatial dimension.

Aside from the baryon number also, the flow of energy is considered in the hydrodynamic description of the time evolution. The hydrodynamic energy–momentum-flow equation, is

$$f^\nu \equiv \frac{\partial T^{\mu\nu}}{\partial x^\mu}, \qquad T^{\mu\nu} = (\epsilon + P)u^\mu u^\nu - g^{\mu\nu}P. \tag{6.6}$$

The form of $T^{\mu\nu}$ we present is suitable for adiabatic (entropy-conserving) flow of matter when the external force density vanishes, $f^\nu \to 0$, a point to which we will return momentarily.

The condition for energy–momentum conservation, Eq. (6.6), involves four equations. One of the equations can be made to look like the conservation equation Eq. (6.5): multiplication by u^ν of Eq. (6.6) yields, using Eq. (6.2),

$$u^\mu \partial_\mu \epsilon + (\epsilon + P)\partial_\mu u^\mu = 0. \tag{6.7}$$

If the pressure $P = 0$, this is the continuity equation Eq. (6.5) for the energy density. To make this obvious, we write

$$\boxed{\frac{\epsilon + P}{\epsilon}\partial_\mu u^\mu = -\frac{1}{\epsilon}\frac{d\epsilon}{d\tau}.} \tag{6.8}$$

For $P \neq 0$, the energy flow ($u^\mu \epsilon$) is not conserved. For $P > 0$, there is a transfer of the energy content of matter to the kinetic energy of the flow of matter. The expanding matter cools. In the rare situation that $P < 0$ (see section 3.5), the transfer of energy goes from kinetic energy of flow back to the intrinsic energy density ϵ.

Equation (6.7) is equivalent to Eq. (1.17), which we recognize using Eq. (6.5),

$$\frac{1}{\epsilon + P}\frac{d\epsilon}{d\tau} = \frac{1}{\rho_i}\frac{d\rho_i}{d\tau}, \quad \frac{d\epsilon}{\epsilon + P} = d(\ln \rho_i) = -3\frac{\dot{R}}{R}, \tag{6.9}$$

noticing that the local density scales with $\rho \propto 1/V \propto 1/R^3$.

https://doi.org/10.1017/9781009290753.009 Published online by Cambridge University Press

The other three equations which follow from Eq. (6.6) determine the velocity field $\vec{v}(\vec{x},t)$, Eq. (6.1),

$$\boxed{\frac{\partial\vec{v}}{\partial t}+(\vec{v}\cdot\vec{\nabla})\vec{v}=-\frac{1-v^2}{\epsilon+P}\left(\vec{\nabla}P+\vec{v}\,\frac{\partial P}{\partial t}\right),} \tag{6.10}$$

which form is obtained for the three spatial components $i=1,2$ and 3 in Eq. (6.6). Naturally, a solution of the hydrodynamic equations can be obtained only when the equation of state $P(\epsilon)$ is known, or equivalently, $\epsilon(T)$ and $P(T)$ are given.

As we have noted, the hydrodynamic-flow equation Eq. (6.6) conserves entropy. To show this, we consider again a contraction with u_ν of the hydrodynamic equations, but this time, we proceed in a different fashion. In the following the sum over the repeated index i is implied, which denotes more than one conserved particle number; in the simplest case, it is the baryon number,

$$\begin{aligned} u_\nu(\partial_\mu T^{\mu\nu}) &= \partial_\mu u^\mu(P+\epsilon)-u^\mu\partial_\mu P \\ &= \partial_\mu u^\mu(T\sigma+\mu_i\rho_i)-u^\mu\partial_\mu P, \end{aligned} \tag{6.11}$$

where we have used the Gibbs–Duham relation, see Eq. (10.26). After some reordering of Eq. (6.11), we obtain

$$0=T\partial_\mu(\sigma u^\mu)+\mu_i\partial_\mu(\rho_i u^\mu)+\sigma u^\mu\partial_\mu T+\rho_i u^\mu\partial_\mu\mu_i-u^\mu\partial_\mu P. \tag{6.12}$$

The first term is the conservation of entropy flow which we are looking for,

$$\boxed{\frac{\partial\sigma^\mu}{\partial x^\mu}=0,\quad \sigma^\mu=\sigma u^\mu,} \tag{6.13}$$

and thus other remaining terms in Eq. (6.11) should cancel out. The second term is the conservation of current flow, Eq. (6.3); it vanishes naturally.

The last three terms in Eq. (6.11) all contain the total proper time local derivative, Eq. (6.4). After multiplication with $d\tau$, we see that, for them to cancel out, we must have

$$0=\sigma\,dT-dP+\rho_i\,d\mu_i\rightarrow 0=S\,dT-V\,dP+b_i\,d\mu_i. \tag{6.14}$$

On multiplying by the volume V, we find the relation on the right-hand side. A more convenient way to consider Eq. (6.14) is

$$0=d(TS-PV+b_i\mu_i)-(T\,dS-P\,dV+\mu_i\,db_i), \tag{6.15}$$

where, according to the Gibbs–Duham relation Eq. (10.26), the left parenthesis is just dE; hence, we recognize Eq. (6.15) as the first law of thermodynamics, Eq. (10.12), which proves Eq. (6.13).

https://doi.org/10.1017/9781009290753.009 Published online by Cambridge University Press

For a more complete discussion of the relativistic hydrodynamics, we refer the reader to the monograph by Csernai [98], as well as introductory sections in *Gravitation and Cosmology* by Weinberg [267], who considers generalization of $T_{\mu\nu}$ with dissipative terms. A generalization of the adiabatic hydrodynamic expansion to include production of entropy has recently been proposed [114].

6.3 The evolution of matter and temperature

In our following discussion, we consider a reduction of Eq. (6.8). Introducing the velocity of sound,

$$\boxed{\frac{1}{v_{\rm s}^2} \equiv \left.\frac{d\epsilon}{dP}\right|_{S=\text{constant}},} \tag{6.16}$$

we obtain

$$\frac{d\epsilon}{d\tau} = \frac{d\epsilon}{dP}\frac{dP}{dT}\frac{dT}{d\tau} = \frac{1}{v_{\rm s}^2}\sigma\frac{dT}{d\tau}, \tag{6.17}$$

where we have used, in the limit of an extensive system at fixed chemical potential (here zero), for the entropy density, σ,

$$\sigma \equiv \frac{S}{V} = \frac{dP}{dT}, \tag{6.18}$$

which follows from Eq. (10.16). On substituting Eq. (6.17) into Eq. (6.8), we find

$$\partial_\mu u^\mu = -\frac{T\sigma}{\epsilon + P}\frac{1}{v_{\rm s}^2}\frac{1}{T}\frac{dT}{d\tau}. \tag{6.19}$$

The Gibbs–Duham relation, Eq. (10.26), allows us to write Eq. (6.19) in the form

$$\boxed{\partial_\mu u^\mu = -\frac{1}{1 + (\mu_{\rm b}/T)b/S}\frac{1}{v_{\rm s}^2}\frac{1}{T}\frac{dT}{d\tau}.} \tag{6.20}$$

We have introduced $b/S = \nu_{\rm b}/\sigma$, the inverse of the entropy per baryon, which is a constant of motion in ideal fluid dynamics: ideal flow conserves the entropy content and, of course, the baryon number is also conserved. Moreover, in an ideal gas of quarks and gluons, without a significant intrinsic dimensional scale, the ratio $\mu_{\rm b}/T$ of the two-dimensional statistical variables is also not evolving with proper time. In this case, the velocity of sound, $v_{\rm s}^2 = \frac{1}{3}$, is also exactly constant.

Using the conservation of baryon flow ($\rho_i \to \nu_{\rm b}$ in Eq. (6.5)) on the left-hand side of Eq. (6.20), we obtain:

$$\frac{1}{\nu_{\rm b}}\frac{d\nu_{\rm b}}{d\tau} = \frac{1}{1 + (\mu_{\rm b}/T)b/S}\frac{1}{v_{\rm s}^2}\frac{1}{T}\frac{dT}{d\tau}. \tag{6.21}$$

https://doi.org/10.1017/9781009290753.009 Published online by Cambridge University Press

Equation (6.21) allows an exact integer for $1/v_{\rm s}^2 = \text{constant}$. Considering the relativistic quark matter $1/v_{\rm s}^2 = 3$,

$$\frac{\nu_{\rm b}}{\nu_{\rm b}^0} = \left(\frac{T}{T_0}\right)^{3/\left(1+\frac{\mu_{\rm b}}{T}\frac{b}{S}\right)}. \tag{6.22}$$

Some readers may wonder how it is possible that T, rather than $\mu_{\rm b}$, controls the evolution of the baryon density. This, of course, is just an optical illusion. Namely,

$$\frac{T}{T_0} = \frac{T}{\mu_{\rm b}}\frac{\mu_{\rm b}}{\mu_{\rm b}^0}\frac{\mu_{\rm b}^0}{T_0} = \frac{\mu_{\rm b}}{\mu_{\rm b}^0},$$

where the last equality arises since $T/\mu_{\rm b}$ does not change during the isentropic evolution of the ideal quark–gluon gas. In this case a more palatable way of writing Eq. (6.22) is

$$\frac{\nu_{\rm b}}{\nu_{\rm b}^0} = \left(\frac{\mu_{\rm b}}{\mu_{\rm b}^0}\right)^{3/\left(1+\frac{\mu_{\rm b}}{T}\frac{b}{S}\right)}. \tag{6.23}$$

It is interesting to observe that, for a baryon-dense fireball of quark matter, possibly formed in 10–40A-GeV fixed-target heavy-ion collisions, the deviations from the $\nu_{\rm b} \propto \mu_{\rm b}^3$ law are quite significant. However, at the SPS and RHIC, the initial conditions established assure that this relationship is valid: $S/b > 35$ (the SPS value; it is certainly larger at the RHIC) is seen to be relatively large compared with $\mu_{\rm b}/T$ ($\simeq$1.4 at the SPS and $<$0.1 at the RHIC).

Although we were able to extract the behavior of the baryon density from ideal-flow equations in the case of a relativistic gas of particles, the actual objective, namely the determination of the proper time variation of any of the quantities involved, has not been accomplished. We will obtain $T(\tau)$ in a very special, but interesting case, in the next section.

6.4 Longitudinal flow of matter

A special case of interest is the reaction picture invoking a rapid flow of matter along the collision axis, the so-called Bjørken scenario [73]. For this simple picture of the reaction to apply, we need to assume that

1. the colliding particles had so much energy that the flow of energy and matter after the collision remains unidirectional along the original collision axis; and
2. the transverse extent of the system is so large that the existence of the edge of matter in a direction transverse to the collision axis is of little relevance.

https://doi.org/10.1017/9781009290753.009 Published online by Cambridge University Press

An interesting aspect of this 'punch'-through limit, seen in Fig. 5.2(a), is that the baryon number which is attached to the colliding valence quarks will also be leaving the interaction region, continuing to travel along the collision axis. Even though a trail of energy is deposited in the central rapidity region, the hope is that, at the highest energies, we should be able to recreate the baryon-free conditions of the early Universe.

After the time $\tau_0 = 0.25$–1 fm/c has passed since the initial contact between the Lorentz-contracted nuclear pancakes (the laboratory-frame view), the thermalized matter begins its evolution as indicated in figure Fig. 6.1. Each particle involved in the reaction has at its later freeze-out a 'proper' age τ_f since 'birth':

$$\tau_\mathrm{f} = \int_0^f d\tau, \qquad d\tau^2 = dt^2 - d\vec{x}^{\,2}. \tag{6.24}$$

If all particles move with a constant velocity (e.g., c) along a common longitudinal direction z, and assuming that all particles have the same proper time at freeze-out, in laboratory coordinates the freeze-out time, t_f, and the freeze-out space coordinates, z_f, form a hyperbola,

$$t_\mathrm{f} = \frac{\tau_\mathrm{f}}{\sqrt{1-v_\mathrm{f}^2}}, \qquad z_\mathrm{f} = v_\mathrm{f}\,\frac{\tau_\mathrm{f}}{\sqrt{1-v_\mathrm{f}^2}}, \qquad \tau_\mathrm{f}^2 = t_\mathrm{f}^2 - z_\mathrm{f}^2, \tag{6.25}$$

as shown in the body of Fig. 6.1. The trajectory of each particle is a straight line $z = vt$, leading from the interaction point to the freeze-out location on the hyperbolic, $\tau_\mathrm{f} =$ constant, surface.

The Minkowski space–time evolution of the ultra-relativistic collision is then rather simple: soon after the collision has occurred (see the CM-time snapshots to the left, beginning at the bottom in Fig. 6.1), the baryon number of the nuclei begins to separate (black lines along the light cone in Fig. 6.1), leaving in the intermediate region a trail of energy, presumed to be in the baryon-number-free QGP phase. The nuclei are trailed to right and left by the expansion of the energy they deposited at the instant of collision.

As the distance between the projectile and the target increases, the continued longitudinal expansion of every volume element reduces the local energy density/temperature until it is so low that individual hadrons can emerge (the chemical-freeze-out condition). As we shall see, the temperature will depend only on the proper time, Eq. (6.33), not on the rapidity. Therefore, a phase transition or transformation, as the case may be, and particle freeze-out occurs along given $\tau =$ constant space–time hyperbolas. In the graphic representation in Fig. 6.1, it is assumed that most of the time the QGP phase prevails, with a short period of freeze-out and hadronization, before final-state hadrons free-stream out of the interaction region.

https://doi.org/10.1017/9781009290753.009 Published online by Cambridge University Press

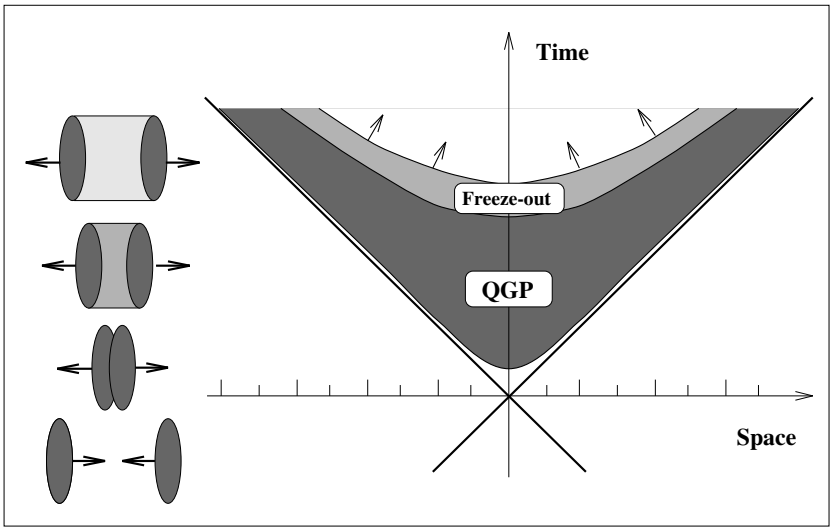

Fig. 6.1. A space–time-image illustration of a heavy-ion collision in the ultra-relativistic (Bjørken) collision limit. Left: Lorentz-contracted nuclei collide and separate as a function of the laboratory time (vertical axis). Right: the light cone establishes the causality limit for the flow of energy, which fills the space–time domain between the separating nuclei.

The spatially central region is obviously at rest in the symmetric CM frame and will emit particles around $y_c = 0$. As we go away from the spatial center, the velocity of the local energy flow under the freeze-out condition increases, reaching the speed of the baryonic matter at the matter-trailing edge (upper right/left-hand edges of the light cone). We see that the rapidity of particles emitted and the relative position in space are correlated. Also, in laboratory time, the earliest particles to be emitted emerge at central rapidity, the latest at projectile–target rapidities, as can be seen in Fig. 6.1.

This discussion suggests that the natural variables in the study of the dynamics of longitudinally expanding matter are the proper time $\tau(t, z)$ which characterizes the parabolas in Fig. 6.1, and the space–time rapidity[‡‡] $y(t, z)$,

$$\boxed{\tau = (t^2 - z^2)^{1/2}, \quad y = \frac{1}{2}\ln\left(\frac{t+z}{t-z}\right),} \tag{6.26}$$

with the inverse relation

[‡‡] The reader is reminded that the variable y is not the spatial coordinate, but the space–time rapidity variable, and that only the spatial coordinate z enters into that which follows.

https://doi.org/10.1017/9781009290753.009 Published online by Cambridge University Press

$$\boxed{t = \tau\,\cosh y, \qquad z = \tau\,\sinh y.} \tag{6.27}$$

We also record that

$$\begin{aligned} \frac{\partial y}{\partial t} &= -\frac{z}{t^2 - z^2}, \quad \frac{\partial y}{\partial z} = \frac{t}{t^2 - z^2}, \\ \frac{\partial \tau}{\partial t} &= \frac{t}{(t^2 - z^2)^{1/2}}, \quad \frac{\partial \tau}{\partial z} = \frac{-z}{(t^2 - z^2)^{1/2}}, \end{aligned} \tag{6.28}$$

and

$$\begin{aligned} \frac{\partial t}{\partial y} &= \tau \sinh y, \quad \frac{\partial t}{\partial \tau} = \cosh y, \\ \frac{\partial z}{\partial y} &= \tau \cosh y, \quad \frac{\partial z}{\partial \tau} = \sinh y. \end{aligned} \tag{6.29}$$

These transformations imply for the volume element that

$$dt\,dz = \tau\,d\tau\,dy. \tag{6.30}$$

The 4-velocity field of some volume element at proper time τ is

$$u^\mu \equiv \frac{dx^\mu}{d\tau} = (\cosh y, 0, 0, \sinh y), \qquad u^2 = 1. \tag{6.31}$$

Equation (6.31) implies that

$$\partial_\mu u^\mu = \frac{\partial u^0}{\partial t} + \frac{\partial u^3}{\partial z} = \frac{\partial y}{\partial t}\frac{\partial \cosh y}{\partial y} + \frac{\partial y}{\partial z}\frac{\partial \sinh y}{\partial y} = \frac{1}{\tau}. \tag{6.32}$$

All these relations become considerably more complex when one allows for flow in the transverse direction. For a velocity field including transverse cylindrical flow see Eq. (8.20).

We will now describe the Bjørken 'scaling' solution for the $(1 + 1)$-dimensional hydrodynamics [73]. The discussion above Eq. (6.26) suggests that one ought to use space–time rapidity and proper time as variables when one is considering a one-dimensional relativistic hydrodynamic model. We substitute Eq. (6.32) into Eq. (6.20) and obtain ($\mu_{\rm b} \simeq 0$)

$$\boxed{\frac{v_{\rm s}^2}{\tau} = -\frac{1}{T}\frac{dT}{d\tau}.} \tag{6.33}$$

This important result allows us to understand how fast the temperature is changing during the 'scaling' one-dimensional hydrodynamic evolution described. We encountered a related result in the study of the adiabatic (isentropic) expansion, see section 1.4.

Perhaps the most cited equation of $(1 + 1)$-dimensional hydrodynamics arises when, in Eq. (6.8), we use Eq. (6.32) (see Eq. (21) in [73]):

https://doi.org/10.1017/9781009290753.009 Published online by Cambridge University Press

$$\boxed{\frac{\epsilon + P}{\tau} + \frac{d\epsilon}{d\tau} = 0.} \tag{6.34}$$

For $\epsilon(T)$ and $P(T)$, this implies that T is a function of τ, but not of y. This important result originates from the assumption that the proper time τ of a fluid volume element is as given in Eq. (6.26), and it is in particular independent of the transverse coordinates.

For a (nearly) relativistic gas $v_s^2 \lesssim \frac{1}{3}$, and the decrease of the temperature is slow. Explicitly, integrating Eq. (6.20), we obtain, assuming that the velocity of sound changes slowly,

$$T = T_0 \left(\frac{\tau_0}{\tau}\right)^{v_s^2}, \tag{6.35}$$

where the initial temperature T_0 is established at an initial (proper) time τ_0, at which local thermal equilibrium has been established and the isentropic hydrodynamic expansion begins. In order to decrease the temperature by a factor two, we need the time $\tau \simeq 8\tau_0$.

In a more realistic evolution of a fireball, which allows for transverse expansion, the expansion cooling is faster [58, 163]; see section 6.2. On the other hand, one also must allow for a less than fully relativistic sound velocity. The properties of the equation of state obtained on the lattice suggest that, in the vicinity of the phase transition, i.e., for $T < 2T_c$, there are significant deviations from ideal-gas behavior. A seemingly small change in v_s matters: we note that, when $v_s \simeq 0.5$ (recall that $1/\sqrt{3} \simeq 0.58$), for the scaling solution Eq. (6.35), the time needed to decrease the temperature by a factor of two increases two-fold to $\tau \simeq 16\tau_0$.

7 Entropy and its relevance in heavy-ion collisions

7.1 Entropy and the approach to chemical equilibrium

Entropy is a quantity characterizing the arrow of time in the evolution of a physical system – in every irreversible process the entropy increases. In elementary interactions, and in particular those involving relativistic collisions of two large atomic nuclei, there is considerable production of particles and hence of entropy. A number of questions arise naturally in this context:

1. When and how is entropy produced in a quantum process, such as a nuclear collision?
2. How is production of hadronic particles related to production of entropy?
3. How does one measure the entropy produced in the reaction?

https://doi.org/10.1017/9781009290753.009 Published online by Cambridge University Press